Enhancement of fracture toughness in secondary bonded CFRP using hybrid thermoplastic/thermoset bondline architecture

Contents lists available at ScienceDirect

Composites Science and Technology

journal homepage: http://ees.elsevier.com

Enhancement of fracture toughness in secondary bonded CFRP using hybrid thermoplastic/thermoset bondline architecture

A. Yudhanto [a], M. Almulhim [a], F. Kamal [a], R. Tao [a], L. Fatta [a], M. Alfano [b], G. Lubineau [a,*]

[a] King Abdullah University of Science and Technology (KAUST), Physical Science and Engineering Division, COHMAS Laboratory, Thuwal, 23955-6900, Saudi Arabia
[b] Department of Mechanical, Energy and Management Engineering, University of Calabria, 87036, Rende, CS, Italy

ARTICLE INFO

Keywords
A. Adhesive joints
A. Laminate
B. Fracture toughness
B. Interface
B. Delamination

ABSTRACT

Structures made of carbon fiber-reinforced polymer (CFRP) can be assembled using adhesive bonding. However, such bonding is prone to brittle delamination, and a method to improve delamination resistance is desirable. Here, we propose a technique to introduce crack-arrest features that increase the R-curve response by engineering the adhesive bondline/interface. We specifically designed a wavy net-like thermoplastic insert that was embedded into the thermoset adhesive bondline where the new mechanisms of energy dissipation were generated. We demonstrate that the technique is effective at improving mode I fracture toughness of secondary bonded carbon/epoxy by more than 400%. The hybrid thermoset/thermoplastic bondline architecture was carefully tailored to achieve its best performance. We demonstrate that introducing porosities in the adhesive bondline (by adding a limited amount of thermoset adhesive) further improves the fracture toughness. This toughness improvement originates from the extrinsic toughening of the crack-arrest feature, which is enabled by the insert ductility and microstructures (via strand formation, anchoring and stretching).

1. Introduction

Carbon fiber-reinforced polymer (CFRP) composites have been increasingly used to fabricate aircraft parts requiring high specific strength (or stiffness) [1,2]. The parts made of CFRP are typically bonded by co-curing, co-bonding or secondary bonding. In the secondary bonded parts, the joining technique of two or more elements that have been independently cured can be carried out using bolt/rivet (mechanical fastening), adhesive (bonding), or a combination of both [3,4]. However, bolting/riveting usually introduces geometrical perturbation (e.g., holes) in CFRP that increases to a high stress concentration [5], possibly leading to bearing failure due to micro-buckling and delamination [6]. In contrast, adhesive bonding preserves more uniform stress along the bonded area [7]. Adhesive bonding also reduces manufacturing cost by eliminating costly machining steps needed for bolting/riveting [2], and thus represents a promising approach for bonded repair [1]. However, secondary bonded CFRP typically fails by brittle delamination at the adherend-adhesive interface and adhesive failure, resulting in a catastrophic failure [8]. The performance and failure of secondary bonded composites are highly dependent upon surface treatments [9–11], adhesive types (rubbery or rigid) [12], joint designs [12], structural complexity [13], and environmental conditions [14]. Therefore, a method is required to enhance the delamination resistance of secondary bonded CFRP, and to promote an increasing R-curve response so that a ductile response is guaranteed, which can act as a crack-stopping feature and be implemented at the final stage of integration [3,15].

Methods for improving delamination resistance include stitching [16,17], z-pinning [18] and interleaving [19–21]. These methods, however, induce architectural and mechanical shortcomings, such as fiber waviness, in-plane stiffness reduction (stitching or z-pinning [17,18]), manufacturing complexity [21], and are mostly applicable for co-cured CFRP rather than secondary bonding. Methods for improving delamination resistance for secondary bonded CFRP, so-called crack-stopping features, include a thermoplastic crack stopper [4], corrugation [22], staples [23], surface interfering [24], X-type arrester [25], formation of adhesive ligament [26], defect introduction [27] or adhesive bondline architecturing [28,29]. Nevertheless, most of these methods also incur manufacturing complexity, except adhesive bondline architecturing. Adhesive bondline architecturing, which consists of introducing a specific heterogeneous morphology either at the adhesive-substrate interfaces or within the adhesive layer, presents a promising method since it is easily implemented, tailorable, effective (providing sufficient bridging traction for improving delamination resistance), and applicable for bonded repair (latest stage of implementation). In fact, very promising results have been obtained recently by in-

* Corresponding author.
E-mail address: gilles.lubineau@kaust.edu.sa (G. Lubineau)

https://doi.org/10.1016/j.compscitech.2020.108346
Received 29 January 2020; Received in revised form 27 May 2020; Accepted 6 July 2020
Available online xxx
0266-3538/

troducing patterns in the substrates that improve the adhesion properties of the adhesive-substrate interface [26]. In Ref. [26], the authors show that, although the adhesive layer is a purely bulk thermoset layer, controlling its adhesion with the substrates can trigger new mechanisms of dissipation, such as long-range bridging, that promotes an increasing R-curve response. Instead of patterning the substrates in order to modify the adhesion properties between the adhesive layer and the substrates, another option is to directly pattern the adhesive layer, for example, by inserting a crack-arrest feature inside the adhesive. Although the copper mesh proposed in Ref. [28] effectively improved fracture toughness, it was unfortunately non-stretchable (less ductile) and relatively heavy. The nylon mesh described in Ref. [29] is indeed stretchable, but it was designed to control bondline thickness rather than enhance the fracture toughness of the CFRP joint. Therefore, a design of an adhesive layer (bondline architecture) is still needed that is easy to implement, tailorable (freedom in design), and effective for fracture toughness enhancement for CFRP joint via extrinsic toughening.

Here, we propose the use of a crack-stopping feature consisting of a specifically designed wavy net made of 3D printed nylon that can be embedded into the adhesive bondline of CFRP joints. We employ 3D printing technology that allows us to design the crack-stopping feature in a greater freedom, while the implementation can be rather quick. Our specific design proposed here is an illustration and proof of concept. Certainly, a much more general design can be imagined, and may fall within the same concept. Such a technology has been implemented at improving CFRP's performance by implementing a crack-arrest feature in single-lap joints [30,31] and end-notch flexure configurations [32]. In this paper, we study two key design parameters, namely the wavelength of the net waviness and volume of the adhesive (related to the porosity), in relation to the fracture toughness and the corresponding failure mechanism. We experimentally obtain the basic thermal and mechanical properties of nylon as well as the bonding performance between nylon, epoxy and CFRP. We use these properties, along with the observations of the adhesive morphology, to discuss and understand the design of the hybrid thermoplastic/thermoset adhesive layer. Finally, we show that, based on a double cantilever beam (DCB) test, our concept not only greatly enhances the mode I fracture toughness of secondary bonded CFRP, but also introduces a significant increase in R-curve, which is very promising for the design of efficient crack-arrest features.

2. Experimental details

2.1. Materials and methods

We employed carbon/epoxy (T700/M21 Hexply, Hexcel) for manufacturing the adherends. For the floating roller test (FRT) using CFRP specimens, the stacking sequence of flexible and rigid adherends was [0] and $[0/90/0/90/0]_s$, respectively. For double cantilever beam (DCB) specimens, the stacking sequence was $[0]_8$. We manually stacked T700/M21 prepregs, used peel ply for easy removal [33] and cured the prepregs under vacuum (1 bar) and compressed using a static press (Pinette Emidecau Industries 15T) at 7 bar pressures and 180 °C for 2 h. The heating and cooling rates during processing were set at 3 °C/min. The dimensions of the resulting plate were 300 mm × 300 mm × 2 mm. The adhesive paste used for bonding was two-component epoxy (Araldite 420 A/B, Huntsman) made by a weight mixing ratio of 10:4 (for resin and hardener, respectively). The thermoplastic insert (used in the DCB test) or film (used in the FRT) was made of nylon (polyamide 6 or PA6), and manufactured using a 3D printer (BCN3D Sigma). Basic mechanical properties of T700/M21, Araldite 420 A/B and nylon (PA6, 3D printed part) are given in Table 1. Note that PA6 is much more ductile than Araldite 420, making it a good candidate for an insert.

Table 1
Mechanical properties of carbon/epoxy (T700/M21), epoxy adhesive (Araldite 420 A/B) and nylon (PA6) samples.

Material	Parameter	Unit	Value
Carbon/epoxy (T700/M21)	Longitudinal strength	MPa	2138
	Longitudinal failure strain	%	1.60
	Longitudinal modulus	GPa	135
	Transverse strength	MPa	56
	Transverse failure strain	%	0.63
	Transverse modulus	GPa	8.75
	Poisson's ratio	–	0.29
	Fiber volume fraction	%	60.8
	Void volume fraction	%	2.3
Epoxy (Araldite 420 A/B)	Strength	MPa	29
	Failure strain	%	4.6
	Modulus	GPa	1.5
Nylon (PA6), 3D printed	Strength	MPa	42
	Failure strain	%	27
	Modulus	GPa	1.4

2.2. Surface treatment for adherend

We uniformly treated the CFRP plate of 250 mm × 88 mm dimension used for making four DCB specimens using pulsed CO_2 laser irradiation (PLS6.75 Laser Platform, Universal Laser Systems) to remove the thin epoxy layer from the surface. The laser treatment is a scalable technique for making reproducible treated surfaces [34], and is found to enhance bonding strength [35], joint strength [36] and fracture toughness [37]. The parameters in our laser treatment were adapted from Ref. [33,38]: wavelength = 10.6 μm, fluence = 3.2 J/cm^2, speed = 500 mm/s, pulse frequency = 20 kHz, power = 22.5 J. These parameters could remove the epoxy layer (ablation effect), and produce bare fibers that make a direct contact with bonding adhesive. After the treatment, we cleaned the surface using acetone in an ultrasonic cleaner (Branson 8510) for 30 min, and dried it at 60 °C for 30 min.

2.3. Manufacture of insert

We used a 3D printer (BCN3D Sigma) to print a flat net (0.5 mm diameter) and a weft net (0.3 mm diameter). We used printing parameters that we have optimized in-house: extruder temperature = 245 ◦C, 0.4 mm nozzle diameter, temperature of bed = 75 ◦C, printing speed = 60 mm/s, layer height = 0.1 mm, and infill = 0. To create a wavy insert, we manually weaved the flat net into the weft (see Fig. 1a), creating an insert with 0.8 mm thickness, which then represents the bondline thickness. The design principles of the wavy insert are (i) non-symmetrical with respect to the neutral axis of the bondline to anchor at best on both interfaces and enable the creation of bridging strands; (ii) sufficiently thin to be integrated within the bondline; (iii) practically viable to be manufactured using various techniques. We tested inserts with two different wavelengths λ, i.e., short wavelength (λ = 20 mm), long wavelength (λ = 40 mm); see Fig. 1b for λ = 40 mm. The spacing between two weft lines is 10 mm and 20 mm to make short and long wavelengths, respectively. The unit cell and the net dimension are shown in Fig. 1c.

2.4. Thermal characterization methods

We used thermogravimetric analysis (TGA) using Netzsch 449F1 to identify the initial decomposition temperature and total mass change of nylon (PA6). We inserted 15 mg of pristine PA6 into a metallic crucible, heated the sample from 25 to 1000 ◦C at 10 ◦C/min, and

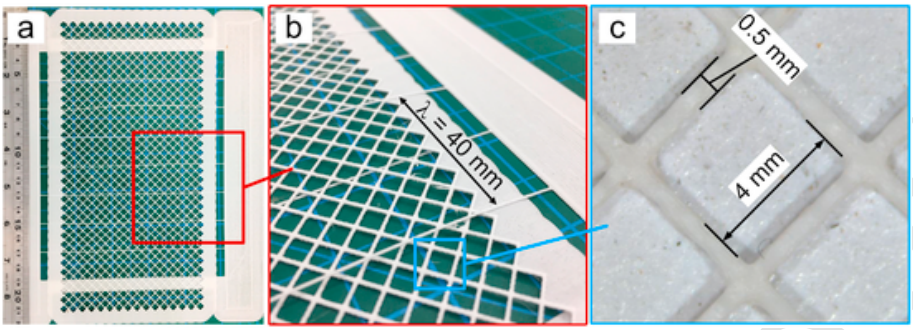

Fig. 1. 3D printed nylon insert: (a) woven insert to be embedded in DCB specimen, (b) wavelength λ between two weft lines, (c) dimension of unit cell of the net insert.

cooled down to 25 ◦C at 10 ◦C/min with the aid of liquid nitrogen. We also performed differential scanning calorimetry (DSC) using Netzsch STA to reveal the onset and endset of melting temperatures of PA6. We inserted 3.5 mg of pristine PA6 into a metallic crucible and heated the sample from 25 to 220 ◦C at 10 ◦C/min in order to remove the thermal history (first cycle), and subsequently reduced the temperature to 25 ◦C at 10 ◦C/min (second cycle). In addition, we used a Linkam heating stage (HFS-600E-PB4) to capture the physical melting process of PA6 in situ. We subjected 3D-printed filament (0.8 mm diameter) with 5 g weight to temperatures of 25, 60, 180, 200 and 210 ◦C (heating rate = 100 ◦C/min; dwell time = 1 min), while we observed the morphological changes using 10× optical microscope. In addition, we also subjected rectangular samples (30 mm × 10 mm) to temperatures of 25, 70, 180, 200 and 210 ◦C in a Memmert oven for 15 min, and observed any discoloration in the nylon using optical microscope (Leica).

2.5. FRT method

It is important to note that performing floating roller test (FRT; ASTM D3167 [39]) prior to DCB testing could provide two benefits: (i) simple specimen preparation and relatively easy to do, (ii) quick indication of whether the insert would strongly attach to the adhesive or not. We performed FRT to measure the peel strength between flexible and rigid adherends with two configurations: (i) CFRP-epoxy-CFRP (reference), (ii) epoxy-nylon. In the CFRP-epoxy-CFRP configuration, the flexible CFRP adherend had dimensions of 250 mm length, 25 mm width, and 0.34 mm thickness, while the rigid CFRP had dimensions of 140 mm length, 25 mm width, and 2.54 mm thickness. The epoxy bondline was Araldite 420 A/B with 329 μm thickness. In the epoxy-nylon configuration, we employed 3D-printed nylon films. The dimensions of epoxy adherend were 185 mm length, 12.5 mm width, 3 mm thickness with a 50 mm initial crack, while those of nylon were 250 mm length, 12.5 mm width, and 0.5 mm thickness. Our 3D printing process (filament deposition modeling) produced films with smooth and rough surfaces. The smooth surface was the part peeled-off from the glass bed, whereas the rough surface was the one directly exposed to the open air. Therefore, we prepared epoxy/rough-nylon and epoxy/smooth-nylon specimens to gain a clear indication about how much the surface finish influences the adhesion. We directly bonded the nylon film to the epoxy that was still in its liquid state, and both were cured at 60 ◦C for 195 min. The FRT test was performed using Instron 5944 (2 kN load cell) at a loading speed of 152 mm/min.

2.6. DCB test method

Fig. 2 shows the schematic of the DCB specimen based on ASTM D5528 [40]. The DCB specimen is 250 mm in length and 20 mm in width. We bonded two CFRP adherends (2 mm thick each) using epoxy adhesive (Araldite 420 A/B) with bondline thickness of 0.8 mm. The total thickness of the specimen was 4.8 mm. To integrate the insert, we first applied the adhesive to the 250 mm × 88 mm treated CFRP adherend. We prepared samples with 14 g (non-saturated amount) and 30 g (saturated amount) adhesive weight since the adhesive amount affected the porosity level and strand formation. We then laid the wavy insert on one of the CFRP adherends that had a thin adhesive layer. We used two inserts with short wavelength (λ = 20 mm) and long wavelength (λ = 40 mm). A non-sticky polyethylene film (80 μm thickness) was inserted between CFRP adherends to create a starter crack of 60 mm, which provided an initial crack length a_0 of 50 mm (measured from the loading pin). We subsequently laid another CFRP adherend that also had a thin adhesive layer, and stacked the sample under 10 kg weight. Curing was performed at 60 °C for 195 min (15 min under vacuum, 180 min at ambient conditions). Once the adhesive bondline was cured, we cut the plate into individual DCB specimens. The specimen configurations are summarized in Table 2. We attached two loading blocks (aluminum) to the upper and lower parts of the specimen to enable the connection with the load cell of Instron 5882 (500 N capacity). We performed the DCB test continuously with a loading speed of 2 mm/min, while we determined the crack length (a) using a Canon EOS 1DS Mark III digital camera that was equipped with Sigma EX lens (up to 300 mm). The identification of the crack tip was carefully done by tracking the position and propagation of the crack using the high-resolution remote viewer installed in the PC. Indeed, as has been noted in Ref. [41], the presence of voids in the adhesive bondline affects the fracture toughness due to the void geometry, crack blunting and determination of the crack tip. In our case, when the crack was entering a void (of a rectangular or elliptical shape) the tip of the void was considered the 'crack tip'. This conservative approach considers that the void length is added to the preceding crack length, thus slightly modifying the apparent fracture toughness. We determined the crack tip using this technique consistently across all specimens with inserts. Load (P) and displacement (δ) data was recorded using the Bluehill software. We tested at least four samples to obtain G_{Ic} vs. crack length (R-curve). Mode I fracture toughness G_{Ic} was calculated using the compliance calibration (CC) method with correction factors of F (large-displacement correction) and N (loading-block correction) [40,42]:

$$G_{Ic} = \frac{nP\delta}{2Ba}\cdot\frac{F}{N} \tag{1}$$

where B is the specimen width, a is the crack length, n is the exponent of the slope between $\log(C/N)$ and $\log(a_i)$, where C is δ_i/P_i. The corrections factors of F and N are given as follows:

$$F = 1 - \frac{3}{10}\left(\frac{\delta}{a}\right)^2 - \frac{3}{2}\left(\frac{\delta t}{a^2}\right) \tag{2}$$

$$N = 1 - \left(\frac{L'}{a}\right)^3 - \frac{9}{8}\left[1 - \left(\frac{L'}{a}\right)^2\right]\left(\frac{\delta t}{a^2}\right) - \frac{9}{35}\left(\frac{\delta}{a}\right)^2 \tag{3}$$

where L' is the horizontal distance between center of the loading

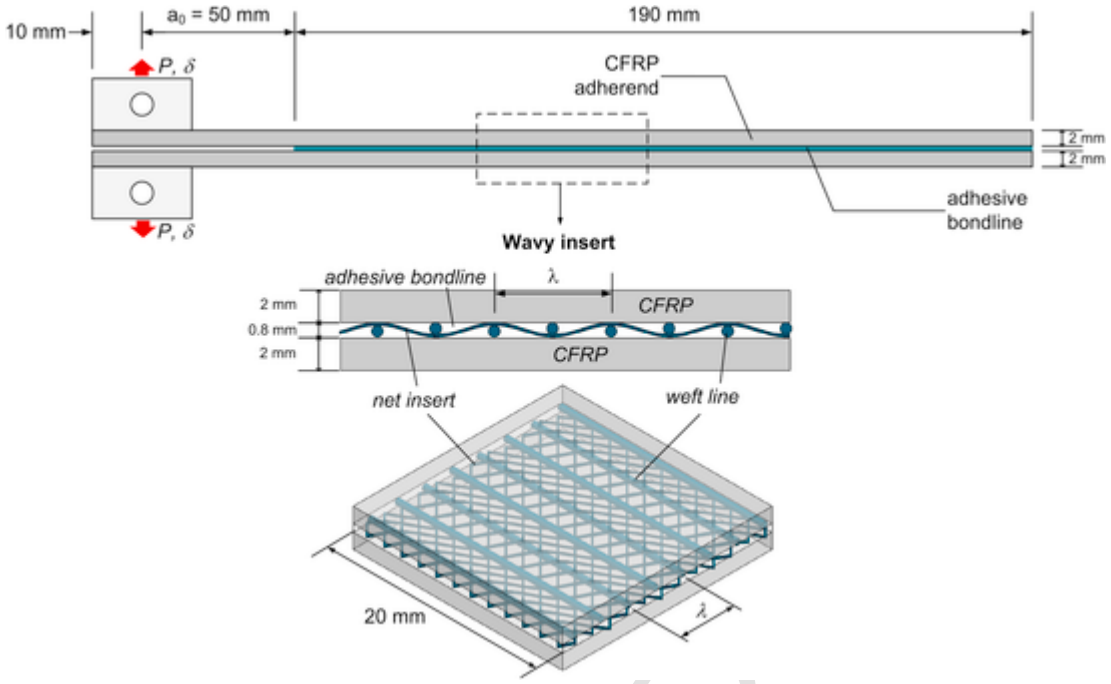

Fig. 2. Schematic of the double cantilever beam with wavy insert within the adhesive bondline.

Table 2
Specimen types for DCB test.

Configuration	Specimen code	Wavelength λ (mm)	Adhesive application
Without insert	C (control)	–	Saturated (30 g)
With insert	L20-W14	20	Non-saturated (14 g)
With insert	L20-W30	20	Saturated (30 g)
With insert	L40-W14	40	Non-saturated (14 g)
With insert	L40-W30	40	Saturated (30 g)

pin and edge of the loading block (L' = 10 mm), while t is the vertical distance between the center of the loading pin and the mid-plane of the substrate (t = 4 mm). Correction factor F is especially important in specimens with inserts since their ratio of opening displacement and crack length (δ/a) is above 0.4 when the crack length was exceeding 125 mm [42].

2.7. X-ray micro-computed tomography

We used X-ray micro-computed tomography (micro-CT, XTH 225, Nikon) to quantify the porosity of the adhesive bondline in DCB specimens with an insert. First, we scanned the specimen with following parameters: beam voltage = 60 kV, beam current = 125 μA, exposure time = 200 ms, frame average = 4, angular step = 0.12°, projection number = 3000, detector resolution = 1910 × 1524, voxel size = 18.2 μm. Subsequently, we reconstructed the projection images using CT Pro 3D (Nikon) software to build a volumetric image. We performed a post-analysis of the 3D images and sliced surfaces using *imageJ*. In addition, we used Avizo software to generate a 3D image of the DCB specimen that we tested halfway in attempt to visualize the internal condition (failure mode) of the bondline.

3. Results and discussion

3.1. Thermal characteristics of nylon

We analyzed the thermal characteristics of the insert material as a guide to ensure safe conditions during the secondary bonding process. The TGA result displayed in Fig. 3a shows that nylon experienced mass degradation (decomposition) at 300 ◦C, below which it is thermally stable. The DSC thermogram depicted in Fig. 3b shows that nylon started to melt at 183 ◦C (melting onset) and was completely melted at 202 ◦C (melting endset). The in situ observation using Linkam heating/cooling stage confirmed that nylon was melting between 200 and 210 ◦C (Point D and E in Fig. 3c). However, nylon actually began to change color (transforming from being originally white to a yellowish color) at 180 ◦C. The discolored nylon was brittle, reducing its effectiveness as an insert. Thus, the maximum temperature for nylon to be inserted in the bondline is 180 ◦C. Nonetheless, we applied a safety margin, and selected a processing temperature of 60 ◦C to ensure a safe condition for adhesive bonding.

3.2. Peel strength evaluation

The load-displacement curves obtained from FRT tests of CFRP-epoxy-CFRP are shown in Fig. 4a. The average peel strength calculated between 50 and 150 mm is 0.51 ± 0.05 N/mm. This reference value is slightly higher than those reported in Ref. [43] (0.28–0.36 N/mm for various epoxy types). FRT test results of epoxy-nylon bonding shown in Fig. 4b–c indicate that the bonding of nylon-epoxy was stronger than that of CFRP-epoxy, i.e., 1.51 ± 0.74 N/mm (for the smooth interface attached to the epoxy) and 2.46 ± 0.75 N/mm (for the rough interface attached to the epoxy). The strong interlocking between nylon and epoxy was a result of mechanical interlocking of nylon-epoxy [44], and chemical bonding between amide (N–H) groups of the nylon and the epoxide groups of the epoxy [45]. Note that we also evaluated the adhesion of nylon that was directly printed on CFRP (prepreg and cured ones), but we do not report the results here as the adhesion of nylon-CFRP was extremely low or zero. Here, we summarized our finding as follows: (i) a direct printing of nylon on cured CFRP results in a very poor (or even zero) adhesion; (ii) a direct curing of epoxy on the already solid thermoplastic insert results in a reasonably strong thermoset-thermoplastic interface that outperforms the original interface obtained by curing epoxy on cured CFRP. Thus, the best way to introduce a thermoplastic insert between two CFRP adherends is to intro-

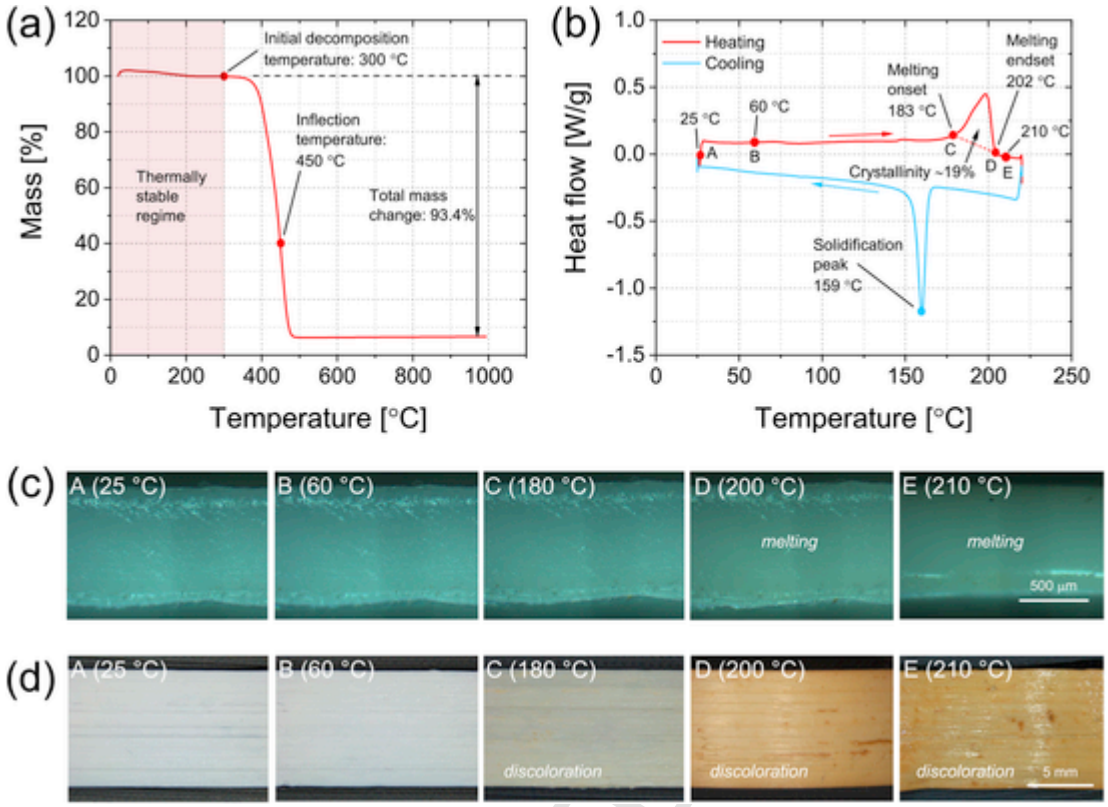

Fig. 3. Thermal characteristics of nylon (PA6): (a) mass-temperature obtained from TGA, (b) heat flow obtained from DSC, (c) melting process in nylon due to temperature increase as observed by Linkam heating stage, (d) discoloration process in nylon due to temperature increase.

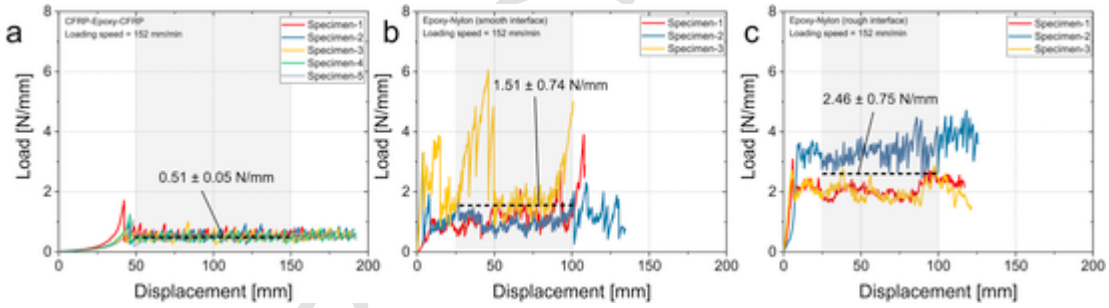

Fig. 4. Load-displacement curves obtained from floating roller tests: (a) CFRP-epoxy-CFRP, (b) epoxy-nylon with smooth nylon interface, (c) epoxy-nylon with rough nylon interface.

duce a layer of epoxy paste, which is then cured in situ, between the insert and the adherend.

3.3. Bondline porosity

We measured the bondline porosity based on the two-dimensional micro-CT images that were processed using *imageJ*. The steps of porosity measurement are given as follows. First, we binarized the micro-CT image (original) obtained from the central portion of the DCB specimen (for example, specimen with $\lambda = 20$ mm and non-saturated adhesive) using *imageJ* in order to transform the original micro-CT image into a monochromatic image. Then, we measured the black regions (porous parts) that have an area size between 0.00001 mm^2 to infinity, and we subsequently normalized it with the total window area to obtain the porosity (in percentage). The results of porosity measurement for all specimens are depicted in Fig. 5 (with corresponding examples of binarized images), showing that specimens with non-saturated adhesive exhibited around 40% porosity, which was relatively higher than that of the saturated adhesive. As we show later, relatively high porosity is useful for triggering the strand formation that bridges the crack, and eventually improves the fracture toughness.

3.4. Enhancement of fracture toughness

Fig. 6a–d shows that the peak load (and the subsequent load bearing capacity) of CFRP specimens with the insert is significantly higher than that without the insert (control specimen). The average peak load of control specimen was 60–70 N, while average peak load of the specimens with insert was around 120 N. Thus, the thermoplastic insert improves the peak load by more than double. However, the peak load is not as sensitive to the amount of adhesive. Fig. 6a–d shows that specimens with saturated and non-saturated adhesive exhibit a similar peak load, suggesting that the initial fracture toughness (G_{IC} initiation) is similar, regardless of the adhesive amount. However, the specimens with saturated adhesive typically failed earlier than those with non-saturated adhesive, indicating that the former has lower G_{IC} propagation than the latter.

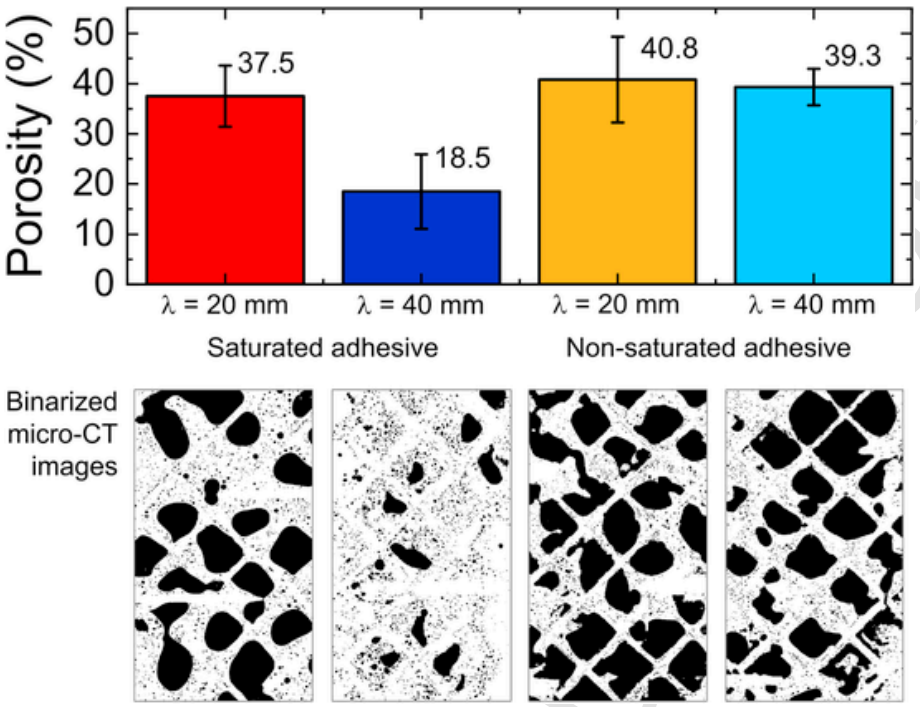

Fig. 5. Porosity level in the adhesive bondline of DCB specimens containing thermoplastic insert with saturated and non-saturated adhesive.

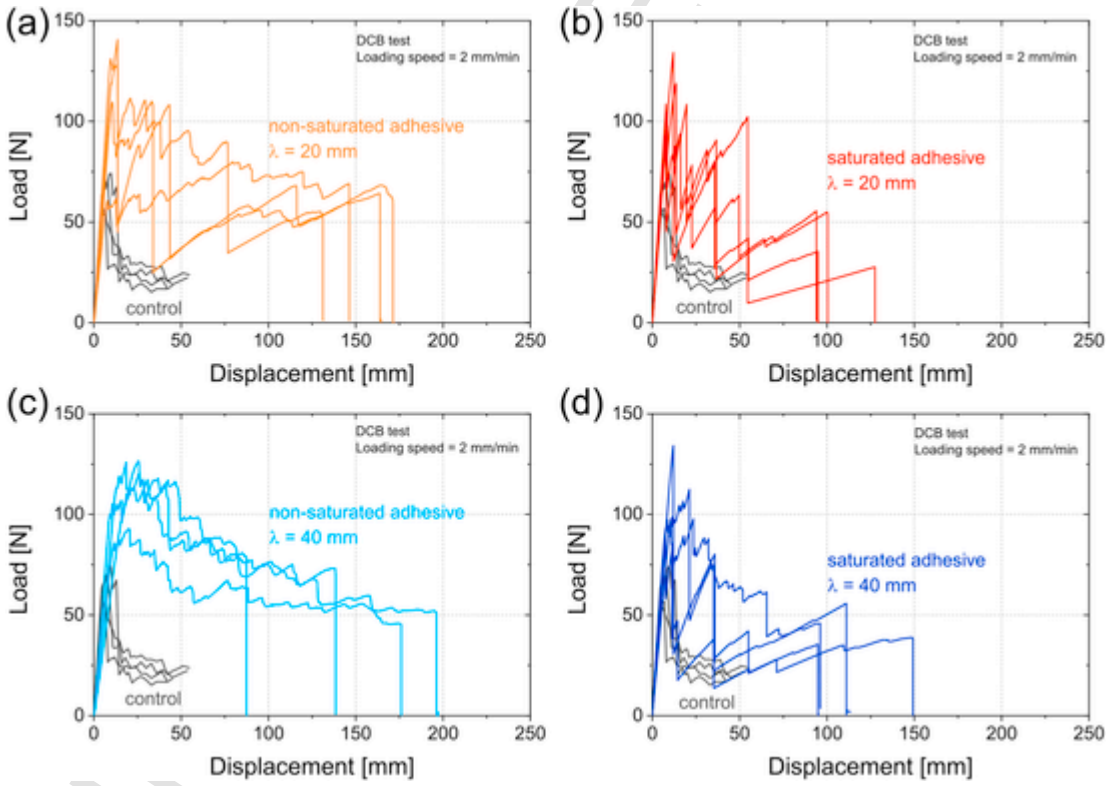

Fig. 6. Load-displacement curves of (a) λ = 20 mm with non-saturated adhesive, (b) λ = 20 mm with saturated adhesive, (c) λ = 40 mm with non-saturated adhesive, (d) λ = 40 mm with saturated adhesive.

G_{IC} plotted against crack length a (R-curve) for specimens with λ = 20 and 40 mm is shown in Fig. 7a and b, respectively. The thermoplastic insert notably enhances fracture toughness (initiation and propagation) by more than 100% compared to the specimens without the insert. Reducing the amount of adhesive improves the fracture toughness by more than 400% with either λ = 20 mm (short wavelength) or 40 mm (long wavelength). In addition, we found that wavelength does not significantly enhance the toughness. This tremendous fracture toughness increase stems from the fact that the insert provides an extrinsic toughening to the CFRP bonded joint.

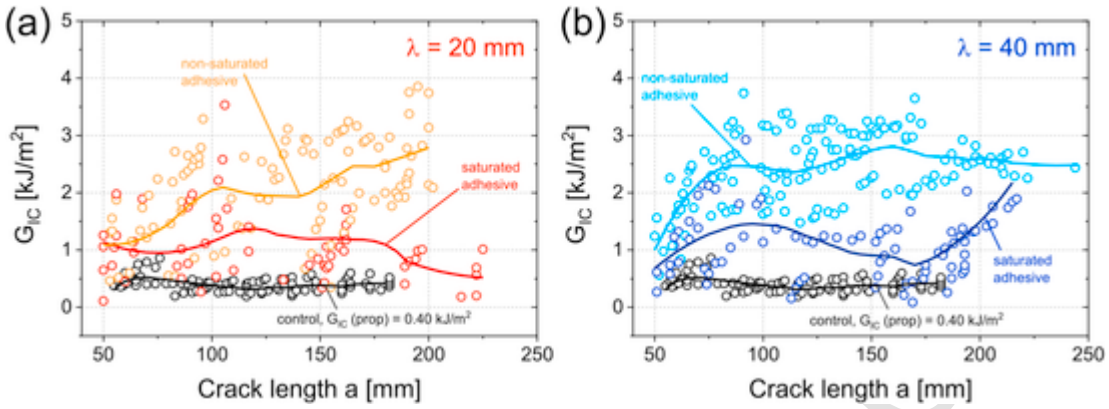

Fig. 7. Comparison among R-curves of specimens with saturated and non-saturated adhesive: (a) λ = 20 mm, (b) λ = 40 mm.

It is noteworthy that, in addition to the DCB test, we also performed the end-notch flexure (ENF) test with a limited number of specimens to measure G_{IIC} of secondary bonded CFRP with a wavy thermoplastic insert. We found that the wavy insert embedded in a bondline with a non-saturated adhesive did not improve G_{IC}. This is due to the fact that the voids existing in the non-saturated adhesive of the ENF specimen, which was apparently useful in Mode I (DCB specimen) for strand anchoring and stretching, acted as a crack initiator in the adhesive bondline under Mode II loading [46]. We believe that implementing saturated adhesive would improve G_{IIC}, and this would be our future evaluation, which may enrich our recent works on the application of laser-based surface patterning strategy on CFRP substrates to improve G_{IIC} [47].

3.5. Crack-bridging mechanism

The fracture toughness enhancement originates from the extrinsic toughening, i.e. crack-bridging mechanism by strands created by the net insert. The number of strands in specimens with saturated adhesive (see Fig. 8a) is minimum because the thermoplastic insert is mostly confined or embedded within the thermoset phase (adhesive bondline). With such a configuration, strands are difficult to form; even if they could be formed, the length of the strands is relatively short. Under a large crack opening, the stretching of such a short strand is so small that it would immediately break along with the epoxy phase. Therefore, the toughness enhancement in specimens with saturated adhesive is rather limited. In contrast, Fig. 8b shows that the specimens with non-saturated adhesive exhibit a large number of bridging strands. The good anchoring of the strands on each side of the joint is promoted by the initial wavy structure of the insert (by breaking the symmetry

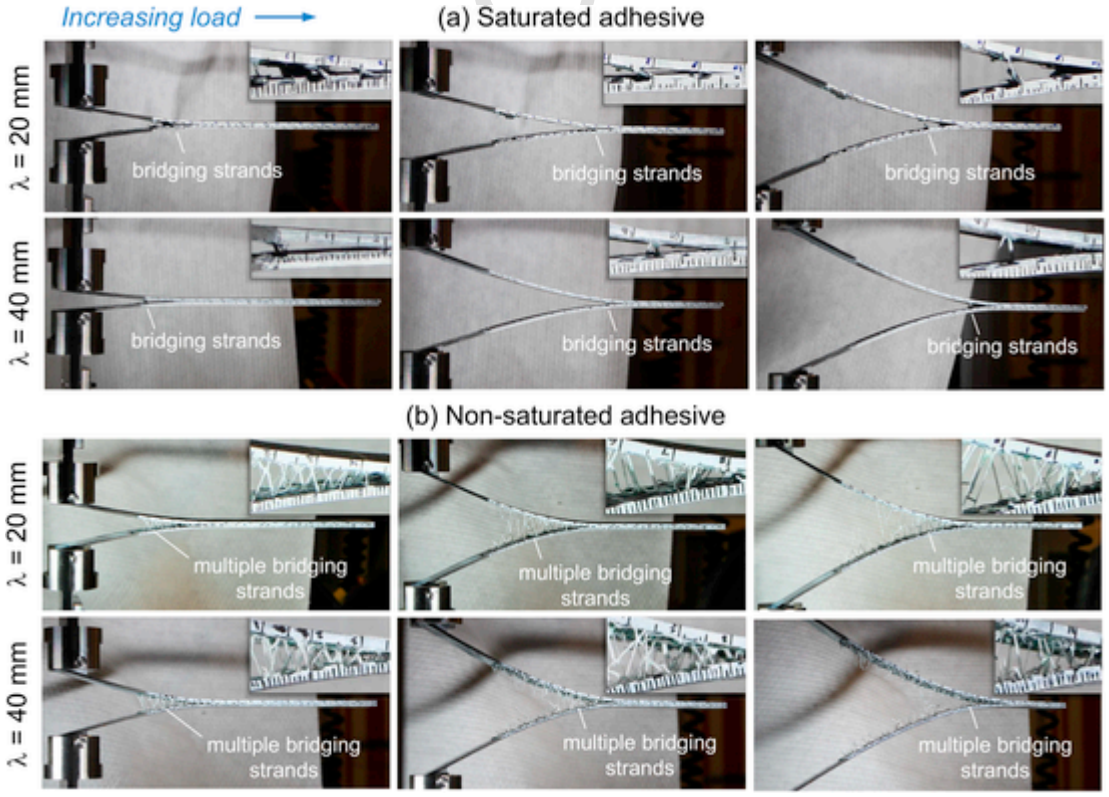

Fig. 8. Effect of using (a) saturated adhesive and (b) non-saturated adhesive on the development of bridging strands in DCB specimens.

of the adhesive layer) and by the good bonding between the nylon and epoxy. Moreover, the thermoplastic strands are mainly embedded in a porous structure that gives enough freedom for the strands to deform and elongate. The ductility of nylon, which is six-fold higher than epoxy, further contributes to the extrinsic toughening due to its stretching capability.

A more detailed mechanism responsible for the extrinsic toughening induced by the insert in specimens with non-saturated adhesive is shown in Fig. 9a–b. As displayed in Fig. 9a, the existence of pores in the initial stage provides some room for the nylon insert to create anchors and strands. Subsequently, the strands were gradually stretched upon loading, while the anchors provided a strong attachment to the adherends. The waviness intentionally created in the insert helped to create more strands between the two adherends. Fig. 9b shows more detailed images of the anchoring, stretching and breaking of the strands. The micro-CT analysis performed on non-failed samples shows that the anchoring typically occurs in the vicinity of the pores. Here, the synergistic combination of the ductile nature of the nylon used for the insert, the mesh-like structure of the insert, the insert waviness, the porosity created by the low amount of adhesive, and strong epoxy-nylon interaction created an excellent crack-arrest feature that significantly improved secondary bonded CFRP.

4. Conclusions

In this work, we proposed novel adhesive bondline architecture by designing and embedding a 3D-printed wavy nylon (thermoplastic) insert into an epoxy adhesive (thermoset) between CFRP adherends. We performed thermal characterization of the 3D printed nylon by utilizing TGA, DSC and Linkam heating stage to determine the range of temperatures for a safe bonding implementation. We performed a floating roller test to clarify that nylon could adhere strongly to the epoxy adhesive. We then performed the double-cantilever beam (DCB) test to measure the mode I fracture toughness of CFRP specimen with and without the embedded insert. We showed that the nylon insert improved the fracture toughness of CFRP bonded specimens by more than 4 times relative to the specimens without the insert. We also found that utilizing non-saturated adhesive (i.e., a less amount of adhesive) provided more space for the strands to operate, thus further enhancing the fracture toughness. The detailed mechanisms for fracture toughness enhancement include: the formation of multiple strands by the insert, anchoring of strands towards the adherend, stretching of strands and ductile fracture of strands. This suggests that a more ductile insert would provide further enhancement of fracture toughness by a tougher crack-arrest feature. It should be noted that our design is indeed tailorable and easy to manufacture thanks to the 3D printing technology. Nevertheless, the selected manufacturing method for the insert here represents a more general technique; other techniques can certainly be adopted, for example, static press using mold or injection molding.

CRediT authorship contribution statement

A. Yudhanto: Conceptualization, Methodology, Supervision, Writing - original draft, Writing - review & editing. **F. Kamal:** Investigation, Data curation, Writing - original draft, Writing - review & editing. **R. Tao:** Investigation, Data curation, Writing - original draft, Writing - review & editing. **L. Fatta:** Investigation, Data curation, Writing - original draft, Writing - review & editing. **M. Alfano:** Investigation, Data curation, Writing - original draft, Writing - review & editing. **G. Lubineau:** Conceptualization, Methodology, Supervision, Writing - original draft, Writing - review & editing.

Declaration of competing interest

The authors declare that they have no known competing financial interests or personal relationships that could have appeared to influence the work reported in this paper.

Acknowledgments

The research funding was supported by King Abdullah University of Science and Technology (KAUST), Office of Sponsored Research (OSR), with award number OSR-2017-CRG6-3388.01. We also thank COHMAS Laboratory Researchers: Mr. Anh-Quan Vu for assisting preliminary FRT test, Mr. Omar Qahtani for preliminary DCB test and 3D printing and Dr. Ahmed Wagih for Mode II test data.

Appendix A. Supplementary data

Supplementary data to this article can be found online at https://doi.org/10.1016/j.compscitech.2020.108346.

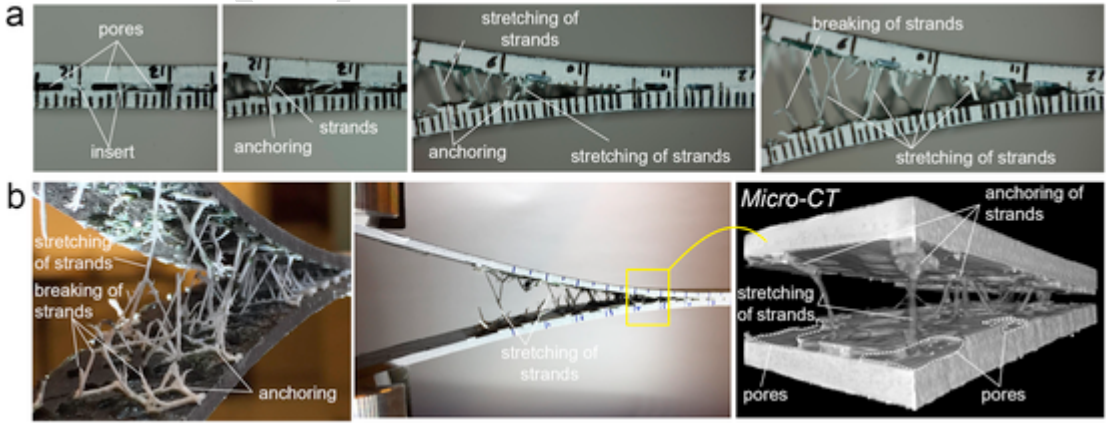

Fig. 9. (a) Bridging mechanism that improves the fracture toughness of specimens with the thermoplastic insert: existence of pores among insert nets, anchoring of insert onto the adherend, formation of multiple strands, stretching of strands, breaking of strands that are still supported by neighboring strands, (b) detailed observation using camera and micro-CT.

References

[1] K B Katnam, L F M Da Silva, T M Young, Bonded repair of composite aircraft structures: a review of scientific challenges and opportunities, Prog. Aero. Sci. 61 (2013) 26–42.

[2] C Soutis, Fibre reinforced composites in aircraft construction, Prog. Aero. Sci. 41 (2005) 143–151.

[3] T Kruse, Bonding of CFRP primary aerospace structures: overview on the technology status in the context of the certification boundary conditions adressing needs for development, The 19th International Conference on Composite Materials, 2013, pp. 5635–5643.

[4] T Löbel, D Holzhüter, M Sinapius, C Hühne, A hybrid bondline concept for bonded composite joints, Int. J. Adhesion Adhes. 68 (2016) 229–238.

[5] T A Collings, The Strength in Multi-Directional of Bolted Joints CFRP Laminates. Technical Report 1380, Ministry of Defence, Aeronautical Research Council, London, 1977.

[6] Y Xiao, T Ishikawa, Bearing strength and failure behavior of bolted composite joints (part I: experimental investigation), Compos. Sci. Technol. 65 (7–8) (2005) 1022–1031.

[7] L F M Da Silva, A Öchsner, R D Adams, Handbook of Adhesion Technology, 2, Springer, 2011.

[8] Astm-D5573, Standard Practice for Classifying Failure Mode in Fiber-Reinforced-Plastic (FRP), 99, ASTM Book of Standards, 2012 (Reapproved):1–18.

[9] N Encinas, B R Oakley, M A Belcher, K Y Blohowiak, R G Dillingham, J Abenojar, M A Martínez, Surface modification of aircraft used composites for adhesive bonding, Int. J. Adhesion Adhes. 50 (2014) 157–163.

[10] K L Mittal, T Bahners (Eds.), Laser Surface Modification and Adhesion, Scrivener Publishing, Wiley, 2015.

[11] R D F Moreira, V Oliveira, F G A Silva, R Vilar, M F S F de Moura, Influence of femtosecond laser treated surfaces on the mode I fracture toughness of carbon-epoxy bonded joints, Int. J. Adhesion Adhes. 82 (2018) 108–113.

[12] A J Kinloch, Adhesion and Adhesives Science and Technology, Springer-Science + Business Media, B.V., 1987.

[13] G A Pappas, J Botsis, Design optimization of a CFRP–aluminum joint for a bioengineering application, Design Science 5 (1–20) (2019).

[14] A Baldan, Adhesively-bonded joints and repairs in metallic alloys, polymers and composite materials: adhesives, adhesion theories and surface pretreatment, J. Mater. Sci. 39 (1 – 49) (2004).

[15] S Sridharan (Ed.), Delamination Behaviour of Composites, Woodhead Publishing Limited, 2008.

[16] A P Mouritz, B N Cox, Mechanistic approach to the properties of stitched laminates, Compos. Appl. Sci. Manuf. 31 (1) (2000) 1–27.

[17] A Yudhanto, G Lubineau, I Aguilar, N Watanabe, Y Iwahori, Damage characteristics in 3D stitched composites with various stitch parameters under in-plane tension, Compos. Appl. Sci. Manuf. 71 (2015) 17–31.

[18] A P Mouritz, Review of z-pinned composite laminates, Compos. Appl. Sci. Manuf. 38 (12) (2007) 2383–2397.

[19] G W Beckermann, K L Pickering, Mode I and Mode II interlaminar fracture toughness of composite laminates interleaved with electrospun nanofibre veils, Compos. Appl. Sci. Manuf. 72 (2015) 11–21.

[20] F Narducci, K Lee, S T Pinho, Interface micro-texturing for interlaminar toughness tailoring: a film-casting technique, Compos. Sci. Technol. 156 (2018) 203–214.

[21] S Minakuchi, K Sawaguchi, K Takagaki, S Niwa, N Takeda, Effect of inter-laminar toughened layers on process-induced strain and deformation of L-shaped composites, Adv. Compos. Mater. 28 (5) (2019) 445–461.

[22] K I Tserpes, G Peikert, I S Floros, Crack stopping in composite adhesively bonded joints through corrugation, Theor. Appl. Fract. Mech. 83 (2016) 152–157.

[23] T Löbel, B Kolesnikov, S Scheffler, A Stahl, C Hühne, Enhanced tensile strength of composite joints by using staple-like pins: working principles and experimental validation, Compos. Struct. 106 (2013) 453–460.

[24] N Sarantinos, S Tsantzalis, S Ucsnik, V Kostopoulos, Review of through-the-thickness reinforced composites in joints, Compos. Struct. 229 (2019) 111404.

[25] S Minakuchi, N Takeda, Arresting crack in composite bonded joint using interlocked fiber feature, ICCM21, Xi'an, China, 2017, pp. 1–6.

[26] R Tao, Xi Li, A Yudhanto, M Alfano, G Lubineau, On controlling interfacial heterogeneity to trigger bridging in secondary bonded composite joints: an efficient strategy to introduce crack-arrest features, Compos. Sci. Technol. 188 (2020) 107964.

[27] M Herráez, N Pichler, J Botsis, Improving delamination resistance through tailored defects, Compos. Struct. 247 (2020) 112422.

[28] K Maloney, N Fleck, Toughening strategies in adhesive joints, Int. J. Solid Struct. 158 (2019) 66–75.

[29] S Heide-Jørgensen, S T De Freitas, M K Budzik, On the fracture behaviour of CFRP bonded joints under mode I loading: effect of supporting carrier and interface contamination, Compos. Sci. Technol. 160 (2018) 97–110.

[30] R Garcia, P Prabhakar, Bond interface design for single lap joints using polymeric additive manufacturing, Compos. Struct. 176 (2017) 547–555.

[31] E Dugbenoo, M F Arif, B L Wardle, S Kumar, Enhanced bonding via additive manufacturing-enabled surface tailoring of 3D printed continuous-fiber composites, Adv. Eng. Mater. 20 (12) (2018) 1–9.

[32] V Damodaran, A G Castellanos, M Milostan, P Prabhakar, Improving the Mode-II interlaminar fracture toughness of polymeric matrix composites through additive manufacturing, Mater. Des. 157 (2018) 60–73.

[33] R Tao, M Alfano, G Lubineau, Laser-based surface patterning of composite plates for improved secondary adhesive bonding, Compos. Appl. Sci. Manuf. 109 (2018) 84–94.

[34] F L Palmieri, M A Belcher, C J Wohl, K Y Blohowiak, J W Connell, Laser ablation surface preparation for adhesive bonding of carbon fiber reinforced epoxy composites, Int. J. Adhesion Adhes. 68 (2016) 95–101.

[35] A Hartwig, G Vit, S Dieckhoff, O-D Hennemann, Surface treatment of an epoxy resin by CO2 laser irradiation, Die Angewandte Makromolekulare Chemie 238 (1996) 177–189.

[36] F Fischer, S Kreling, P Jäschke, M Frauenhofer, D Kracht, K Dilger, Laser surface pre-treatment of CFRP for adhesive bonding in consideration of the absorption behaviour, J. Adhes. 88 (4–6) (2012) 350–363.

[37] M Wetzel, J Holtmannspötter, H J Gudladt, J V Czarnecki, Sensitivity of double cantilever beam test to surface contamination and surface pretreatment, Int. J. Adhesion Adhes. 46 (2013) 114–121.

[38] R Tao, M Alfano, G Lubineau, In situ analysis of interfacial damage in adhesively bonded composite joints subjected to various surface pretreatments, Compos. Appl. Sci. Manuf. 116 (2019) 216–223.

[39] Astm-D3167, Standard test method for peel resistance of adhesives, ASTM Book of Standards 10 (1–4) (2017).

[40] Astm-D5528, Standard Test Method for Mode I Interlaminar Fracture Toughness of Unidirectional Fiber-Reinforced Polymer Matrix Composites, ASTM Book of Standards, 2014, pp. 1–12 03(Reapproved 2007).

[41] Mauro Ricotta, Marino Quaresimin, Talreja Ramesh, Mode i strain energy release rate in composite laminates in the presence of voids, Compos. Sci. Technol. 68 (13) (2008) 2616–2623 (Directions in Damage and Durability of Composite Materials, with regular papers).

[42] B Blackman, A Kinloch, Fracture tests on structural adhesive joints, in: D R Moore, A Pavan, J G Williams (Eds.), *Fracture Mechanics Testing Methods For Polymers, Adhesives And Composites*, Volume 28 of *European Structural Integrity Society*, Elsevier, 2001, pp. 225–267.

[43] S T De Freitas, J Sinke, Test method to assess interface adhesion in composite bonding, Applied Adhesion Science 3 (9) (2015) 1–13.

[44] A Baldan, Adhesion phenomena in bonded joints, Int. J. Adhesion Adhes. 38 (2012) 95–116.

[45] S Deng, L Djukic, R Paton, L Ye, Thermoplastic-epoxy interactions and their potential applications in joining composite structures - a review, Compos. Appl. Sci. Manuf. 68 (2015) 121–132.

[46] N R Abdelal, Effects of Voids on Delamination Behavior under Static and Fatigue Mode I and Mode Ii PhD Thesis University of Dayton, 2013.

[47] A Wagih, R Tao, A Yudhanto, G Lubineau, Improving mode ii fracture toughness of secondary bonded joints using laser patterning of adherends, Compos. Appl. Sci. Manuf. 134 (2020) 105892.